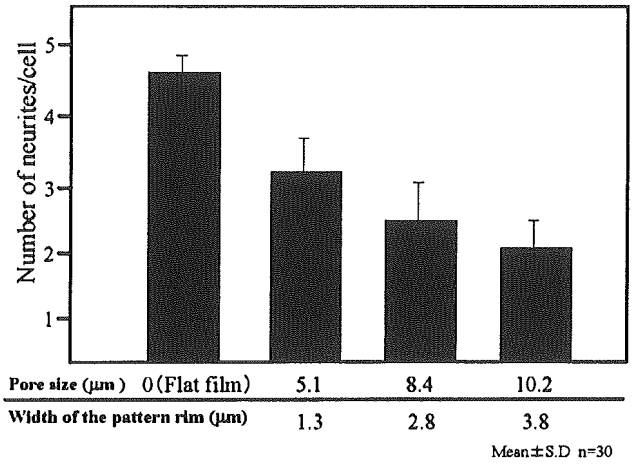

FIG. 5: The number of neurites on flat film and patterned films.

TABLE I: Morphological changes of adhered neurons on PCL film and PCL honeycomb-patterned films.
[a)]Cell morphologies : see Fig. 4.

[a)]Cell morphologies	A	B	C	D	E
Flat film	○				
Honeycomb patterned films					
Pore size (Rim size)					
3.2 μm (1.1 μm)		○			○
5.1 μm (1.3 μm)		○	○		
8.4 μm (2.8 μm)		○	○	○	
10.2 μm (3.8 μm)				○	

films (Figs. 4(a)-(f)). Further, on the patterned film (pattern pore size: ϕ10 μm), each round neuron adhered to the pattern rims. The number and branching of the neurites were reduced compared with those on the flat films. The neurons formed simple network structures on the rims of the patterns. The neurons were round, similar to the morphology of neurons on the flat films (Fig. 4(e)).

Furthermore, we found another specific morphology of neurons on patterned films with a pore size of 3 μm. Neurons formed large spheroid-like round aggregates on these films. The neural aggregates formed large bundles of neurites which extended in the shape of radiation (Fig. 4(f)).

Morphological changes in neurons and formation of lamella structures are likely to depend on the change in pore and rim sizes (Table 1). This suggests that honeycomb patterns act as a guide as well as scaffold for neurons and neurites.

D. Investigation of the number of neurites on the honeycomb-patterned films with varying pore sizes

The honeycomb patterns influenced neurite extension and outgrowth. We investigated the number of neurites per neurons on the PCL flat film and patterned films (5, 8, and 10 μm in diameter). We found that the number of neurites decreased with increasing pore size and rim size of the patterned films (Fig. 5).

Collagen gels and sheets are used as biomaterials for tissue engineering. However, the mechanical strength of these materials is weak, and other polymer substrates are less biodegradable and biocompatible. The advantage of self-organized patterned films is that they are prepared from various biodegradable and biocompatible polymers. The preparation of honeycomb-patterned films dose not require high energy or high cost.

In tissue engineering, it is important to culture cells in 3-D scaffolds [17]. We can culture cells with other cells on both sides of the honeycomb-patterned films. It is believed that the cells can interact with each other via the pores of the patterned films. Moreover, the patterned films can easily be formed in various shapes. With these patterned films, it will be possible to prepare 3-D structures, such as tube, roll, and various multi-layered structures. We can co-culture neurons with glial cells or endothelial cells in these 3-D scaffolds to reconstruct 3-D tissues. The patterned films are candidates for tissue engineering scaffolds.

IV. CONCLUSIONS

We could prepare biodegradable polymer patterned films and control the pore size of the patterned films. Neurons formed neural networks on the patterned films, and the morphologies of cells could be changed by varying pore size of the patterned films. The self-organized honeycomb patterned films are useful biomaterials for neural tissue engineering.

Acknowledgments

This study was supported by Grants-in-Aid from Japan Science and Technology Corporation (JST).

[1] S. Wu, Y. Suzuki, Y. Ejiri, T. Noda, H. Bai, M. Kitada, K. Kataoka, M. Ohta, H. Chou, and C. Ide, J. Neurosci. Res. **72**, 343 (2003).
[2] R. Langer and J. P. Vacanti, Science **260**, 920 (1993).
[3] U. A. Stock and J. P. Vacanti, Annu. Rev. Med. **52**, 443 (2001).
[4] A. M. Green, J. A. Jansen, JPCM. Van der Waerden, and A. F. von Recum, J. Biomed. Mater. Res. **28**, 647 (1994).
[5] A. Mata, C. Boehm, A. J. Fleischman, G. Muschlar, and S. Roy, J. Biomed. Mater. Res. **62**, 499 (2002).
[6] K. Sato, K. Hasebe, M. Tanaka, M. Takebayashi, K. Nishikawa, M. Shimomura, T. Kawai, M. Matsushita, and S. Todo, Int. J. Nanosci. **1**, 689 (2002).
[7] D. Kleinfeld, K. H. Kahler, and P. E. Hockberger, J. Neurosci. **8**, 4098 (1998).
[8] P. Clark, S. Britland, and P. Connolly, J. Cell Science **105**, 203 (1993).
[9] W. Ma, Q. Liu, D. Jung, P. Manos, J. J. Pancrazio, A. E. Schaffner, J. L. barker, and D. A. Stenger, Develop. Brain. Res. **111**, 231 (1998).

[10] H. Tsuji, H. Sato, T. Baba, S. Ikemura, Y. Gotoh, and J. Ishikawa, Nucl. Instr. and Meth. in Phys. Res. B. **166**, 815 (2000).
[11] L. Kam, W. Shain, J. N. Turner, and R. Bizios, Biomaterials **22**, 1049 (2001).
[12] M. E. Manwaring, J. F. Walsh, and P. A. Tresco, Biomaterials **25**, 3631 (2004).
[13] H. Kawasaki, K. Hiraka, S. Nagaoka, and Y. Suzuki, J. Artif. Organs. **7**, 83(2004).
[14] N. Maruyama, T. Koito, J. Nishida, T. Sawadaishi, X. Cieren, K. Ijiro, O. Karthaus, and M. Shimomura, Thin Solid Films **854**, 327 (1998).
[15] T. Nishikawa, R. Ohkura, J. Nishida, K. Arai, J. Hayashi, N. Kurono, T. Sawadaishi, M. Hara, and M. Shimomura, Langmuir **18**, 5734 (2002).
[16] M. Tanaka, M. Takebayashi, M. Miyama, J. Nishida and M. Shimomura, Bio-Med. Mater. Eng. **14**, 439 (2004)
[17] G. A. Silva, C. Czeisler, and K. L. Niece, Science **303**, 1352 (2004).

Available online at www.sciencedirect.com
SCIENCE DIRECT®
ELSEVIER
Colloids and Surfaces A: Physicochem. Eng. Aspects xxx (2006) xxx–xxx
COLLOIDS AND SURFACES A
www.elsevier.com/locate/colsurfa

Topographical control of neurite extension on stripe-patterned polymer films

Akinori Tsuruma [a], Masaru Tanaka [b,c,*], Sadaaki Yamamoto [b,c], Nobuyuki Fukushima [d], Hiroshi Yabu [c,e], Masatsugu Shimomura [c,e]

[a] *Graduate School of Science, Hokkaido University, Kita-Ku N10W8, Sapporo 060-0810, Japan*
[b] *Creative Research Initiative "Sousei" (CRIS), Hokkaido University, Kita-Ku N21W10, Sapporo 001-0021, Japan*
[c] *CREST, Japan Science and Technology Corporation (JST), Honchou 4-1-8, Kawaguchi 332- 0012, Japan*
[d] *Graduate School of Medicine, Hokkaido University, Kita-Ku N15W7, Sapporo 060-8638, Japan*
[e] *Nanotechnology Research Center, Research Institute for Electronic Science, Hokkaido University, Kita-Ku N21W10, Sapporo 001-0021, Japan*

Received 31 July 2005; received in revised form 25 November 2005; accepted 29 November 2005

Abstract

Controlling cell responses to material surfaces is important for tissue engineering. Topographical property on material surfaces can play a crucial role in directing nerve regeneration. We prepared regular stripe-patterned (groove-ridge pattern) polymer film by self-organization in order to control direction of neurite extension. Neural cells from cerebral cortex of embryonic day-14 mice were cultured on the film coated with poly-L-lysine. Here, we describe a complex and unusual contact guidance dependent on the pattern feature size. The neurites grew perpendicular to wide groove of 12.7 μm and wide ridge of 4.3 μm but parallel to narrow grooves (6.1 and 8.4 μm) and narrow ridge (2.2 and 3.6 μm). The neurites sprouted parallel to the narrow groove but uniformly on the wide groove. The emersion of neurites was suppressed and the length of neurites was longer compared with on a flat film. These results are of interest to understanding contact guidance and designing scaffold for neural network formation.

Keywords: Neuron; Micro-patterning; Self-organization; Tissue engineering; Contact guidance

1. Introduction

The central nervous system (CNS) fails to recover following nerve injuries or neurodegenerative diseases. Clinical therapies for CNS damages need surgical end-to-end connection or implantation of conduit materials [1]. A variety of biomaterials have been investigated for neural tissue engineering application. Synthetic materials such as fiber or hydrogels have been used to expand neurites and reconstruct neural network [2,3]. It has been reported that topography of micro-grooves on surface can control direction of neurite outgrowth and neurite development (contact guidance) [4–9]. This surface-contact guidance of neurites on topographical pattern is important to design devices in neural regeneration and to understand axonal formation [9]. The application of micro-fabrication techniques to the topographic designing of polymer surface can provide valuable information for understanding of the contact guidance and materials for neural tissue engineering [10–12]. In previous studies, micro-patterned surfaces were fabricated by lithography and micro-contact printing [13–16]. These techniques are expected to be applied for neural regeneration in the future. However, the techniques require high energy and involve many processes. In addition, materials for scaffolds applicable to the techniques are limited.

We have reported that regular patterns can be formed by casting diluted polymer solution on solid substrates [17–20]. This method has great advantage that the films can be prepared with ease, low-cost and no limitation of materials for scaffold. In this study, we prepared stripe-patterned polymer films on a solid substrate by the method previously reported [20] and cultured neural cells from cerebral cortex of embryonic day-14 mice on the film coated with poly-L-lysine to investigate how these films influence neuronal morphologies and neurite extension in cultures.

* Corresponding author.
E-mail address: tanaka@poly.es.hokudai.ac.jp (M. Tanaka).

0927-7757/$ – see front matter © 2005 Elsevier B.V. All rights reserved.
doi:10.1016/j.colsurfa.2005.11.100

2. Experiment

2.1. Preparation of stripe-patterned polymer films

Stripe-patterned polymer films were prepared with an instrument described in the previous literature (Fig. 1) [20,21]. We prepared poly (ε-caprolactone)/chloroform solution (1 g/L) before casting. Glass plates were overlapped by ca. 4 cm and separated with a narrow gap (200 μm). Then, polymer solution (200 μl) was injected into the gap between two glass plates. The upper glass plate was moved straightly at the velocity controlled from 60 to 100 μm/s (Fig. 1). A thin liquid film of polymer solution was continuously formed from the edge of sliding glass, and the polymer intermittently deposited on the bottom glass following evaporation of solvent at the meniscus. Polymer patterns were observed by optical microscope (BH-2, Olympus, Japan), atomic force microscope (SPA-400, Seiko Instruments, Japan) and scanning electron microscope (S-3500, Hitachi, Japan).

2.2. Preparation of flat polymer films

The polymer solution (poly(ε-caprolactone) (MW 30,000–70,000)/chloroform solution (1 g/L)) was dropped onto a slide glass. The slide glass with polymer layer was spined at 1000 rpm for 30 s by spin coater (MIKASA, 1H-7D).

2.3. Neural cell culture

Neural cells were prepared from the cerebral cortex of embryonic day-14 mice (CLEA Japan, Inc). In brief, the cerebral cortices of embryonic day-14 mice were dissected and the meninges were carefully removed. The tissues were transferred to 15 ml tubes with culture medium containing 55 μM 2-mercaptoethanol and gently triturated with a fire-polished pasteur pipette until most of the tissues were dissociated into single cells. Then, the cell number and viability were measured. The cells were seeded onto the flat film to estimate the population of neural stem cells (NSCs). The neural cells were seeded onto the flat and stripe patterned film at a density of 2.0×10^4 cells/cm^2. They were cultured in serum medium (Opti-MEM (Invitrogen), 10% fetal bovine serum, and 55 μM 2-mercaptoethanol (Invitrogen)) for the first day at 37 °C under a humidified atmosphere of 5% CO_2. After the second day, they were further cultured in serum-free medium (Opti-MEM, B27 supplement, and 55 μM 2-mercaptoethanol). After 5 days culture, morphologies of neurons and neurite extension were observed using scanning electron microscope (SEM) (S-3500, Hitachi, Japan), confocal laser scanning microscope (CLSM) (Fluoview FV 300, Olympus, Japan) and phase contrast microscope (IX 70, Olympus, Japan).

2.4. Preparation of the sample for SEM observation

The cultured cells were fixed with 2.5% glutaraldehyde in phosphate-buffered saline (PBS). They were washed with PBS and water. Subsequently, the samples were dehydrated by washing in increasing ethanol concentrations and then air-dried. The samples were sputtered with platinum.

2.5. Preparation of the sample for CLSM observation

The cultured cells were fixed with 10% formaldehyde in PBS for 30 min at room temperature. The samples were washed with PBS three times for 5 min. They were then incubated in blocking solution (5% goat serum, 0.2% Triton X-100 in PBS) for 1 h. Then, the samples were incubated with mouse monoclonal anti-β-tubulin III (1:500) in PBS for 2 h. After washing with PBS, the samples were incubated with fluorescein isothiocyanate (FITC)-conjugated anti-mouse IgG (1:200) for 2 h. After washing with

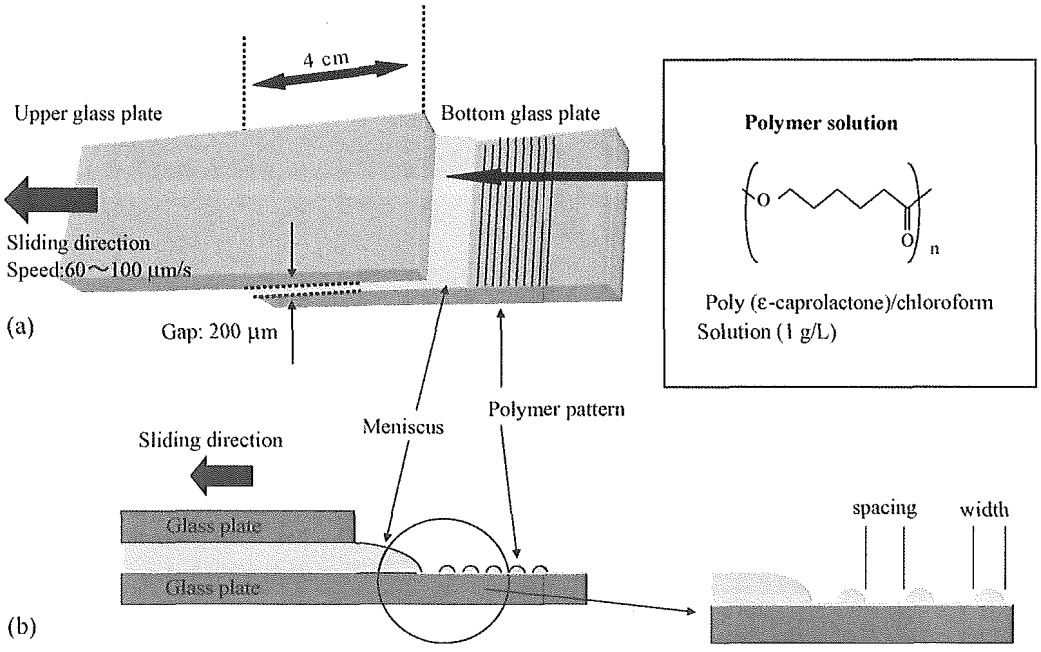

Fig. 1. Schematic images for preparation of stripe-patterned films. (a) Tilt and (b) side view.

PBS and water, the sample were air-dried and then mounted with mounting media for CLSM observation.

3. Results and discussion

3.1. Stripe-patterned polymer films

At a sliding speed of 60, 70 and 100 μm/s, the stripe pattern polymer films were prepared. Width ("ridge") and spacing ("groove") of the substrates were 2.2 and 6.1 μm (sliding speed: 60 μm/s), 3.6 and 8.4 μm (sliding speed: 70 μm/s), and 4.3 and 12.7 μm (sliding speed: 100 μm/s), respectively. The height of the ridges was in the range of 50–100 nm. This type of the periodic deposition is caused by "stick-slip motion," which is often observed in colloidal crystals [22] and is commonly known as the coffee stain phenomenon [23]. Due to evaporation of solvent at the meniscus, polymer was condensed at the edge of solution [20,21]. Increasing local viscosity of polymer solution caused by polymer gelation resulted in pinning of the solution edge at the meniscus. After complete deposition of polymer onto the glass substrate, the pinning stress relaxed and the solution edge moved in the sliding direction like a receding tide until the next pinning.

3.2. Morphologies of neurons and neurites extension on patterned/flat films

Fig. 2 shows morphologies of neurons and extended neurites observed by using SEM, and CLSM. Cells cultured for 5 days on the flat and patterned films were stained with neuron-specific marker, β-tubulin III. Cells were positive for β-tubulin III on the both films, indicating that these cultured cells were differentiated neurons (Fig. 2a and c).

The large difference was noted when comparing the behavior and morphology of neurons on the flat film with those on the patterned films. On the flat film, neurons were round in shape. They extended many branched neurites, and seemed to form neuronal network with random direction of neurite outgrowth (Fig. 2a and b). In contrast, on the patterned film, neurons attached and elongated parallel to the stripes (indicated by arrowheads in Fig. 2c and d). Cells altered their shapes, orientation and direction of neurites extension to align with the stripe-pattern (indicated by arrows in Fig. 2c and d). These results imply that the stripe-pattern affects the orientation of neurite outgrowth, neurite emersion and neurite growth.

3.3. Effect of pattern width ("ridge") and spacing ("groove")

Next, we describe the effects of width ("ridge") and spacing ("groove") of the stripe-patterned polymer film on neurites extension. The morphologies on the patterned films showed complex and unusual contact guidance dependent on the pattern feature size (Figs. 2c and d, 3a and b). Neurites were predicted to be able to extend out of the grooves with height ≤4.7 μm [5]. Unless the neurites are able to extend out of

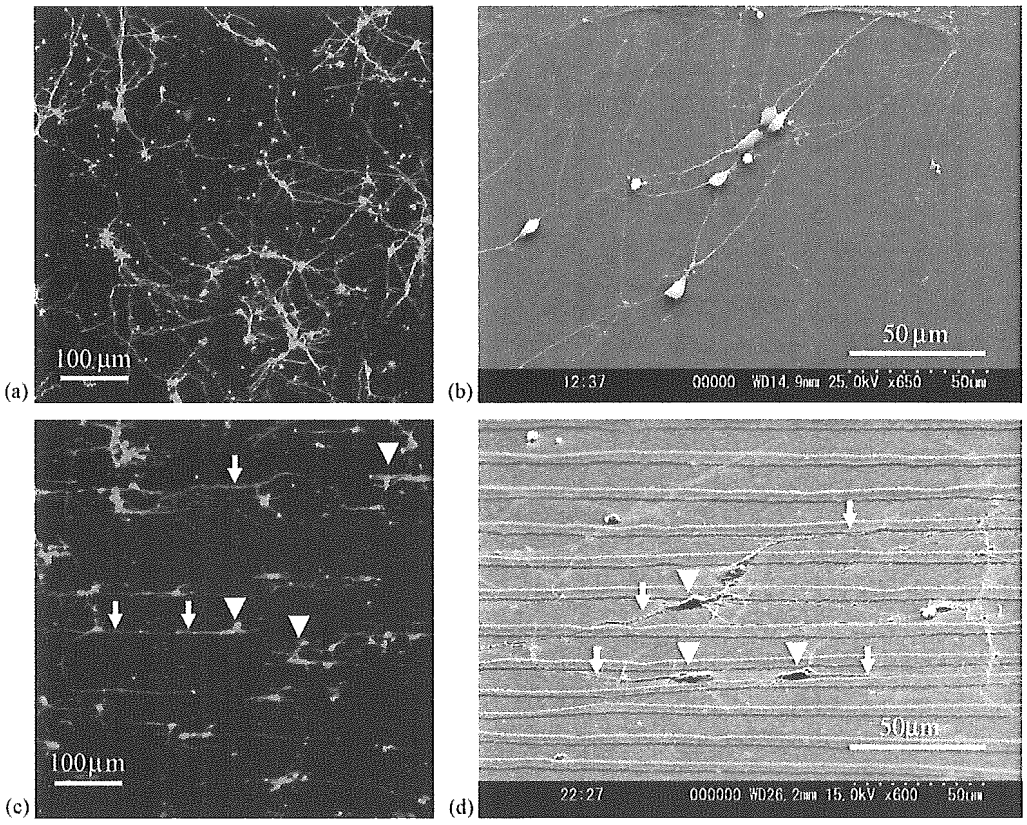

Fig. 2. Morphologies of neurons and neurite extension in SEM and CLSM. (a) Fluorescence image on flat film (staining for β-tubulinIII), (b) SEM image on flat film, (c) fluorescence image on stripe-patterned film (staining for β-tubulinIII) width: 3.6 μm, spacing: 8.4 μm (sliding speed: 70 μm/s) and (d) SEM image on stripe-patterned film. width: 3.6 μm, spacing: 8.4 μm (sliding speed: 70 μm/s).

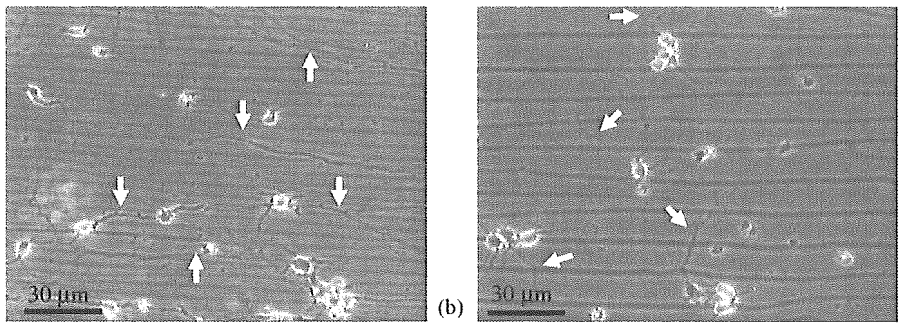

Fig. 3. Morphologies of neurons and neurite extension in phase contrast images on (a) stripe-patterned film, width: 2.2 μm, spacing: 6.1 μm (sliding speed: 60 μm/s) and (b) stripe-patterned film, width: 4.3 μm, spacing: 12.7 μm (sliding speed: 100 μm/s).

the grooves of the stripe-patterned film, a subset of neurons extended neurites in grooves parallel to the axis of the pattern on narrow pattern width and spacing (width: 2.2 μm, spacing: 6.1 μm) (indicated by arrows in Fig. 3a). The narrow patterns determine the site on a cell body where neurites emerged (Fig. 2c and d, and 3a). On wide pattern width and spacing (width: 4.3 μm, spacing: 12.7 μm), most neurites extended across the axis of the pattern (indicated by arrows in Fig. 3b). The number of neurites per a cell body was reduced and the length of neurites was longer on the stripe patterned-films comparing with that on the flat film shown in Fig. 2a and b. These results show that the neurites sense the dimension of regular stripe patterns.

In previous studies, similar parallel and perpendicular contact guidance of neurites has been observed on microgrooved fused quartz substrates in response to stripe-patterned feature dimension and cells. Several hypothesis have been proposed on the mechanism of contact guidance. CNS neuroblasts orient their neurites both perpendicular and parallel to the axis of grating-like structure [4]. Perpendicular orientation is frequently observed when the microstructured grooves have depths between 300 and 800 nm and a width of 1 μm. Embryonic rat hippocampal neurites grow parallel to grooves with height of 1 μm and width of 4 μm, and perpendicular to grooves with height of 130 nm and width of 1 μm on fused quarz [5,6]. *Xenopus* neurites grow parallel to grooves as shallow as 14 nm and as narrow as 1 μm [5]. Recently, neonatal rat dorsal root ganglion neuron was reported to extend neurites that bridged across grooves with no underlying solid support on deep grooves of 50 μm [7]. The cell–cell interaction was supposed to be involved in the bridging of the neurites across grooves. Not only groove width but also ridge width plays an important role in bridge formation. The dependence of contact guidance on the pattern size for neurons from cerebral cortex of embryonic day-14 mice in the present study conflicts that for CNS neuroblasts and embryonic rat hippocampal neurons. The pattern width (ridge width) of the stripe-patterned polymer film in the present study varied companying with the spacing. The neurites might sense both the pattern width and spacing. This might lead to the contact guidance characteristic for the stripe-patterned polymer films by self-organization different from that on microgrooved fused quartz.

The possibilities considered for the mechanism of the perpendicular orientation were proposed such as the extension of a neurite at right angles to the structure by recognition of the physical surface structure of neurite bundles and the involvement of more specific surface molecules on the neurites responsible for the perpendicular contact guidance [4]. Parallel and perpendicular orientation of hippocampal neurites are supposed to utilize different mechanisms [6]. Growth cones of neurite recognize the topography of the surfaces [13,23,24]. The structure of growth cones is critical to neurite guidance and aids in the sensing and exploration of the underlying environment. Further, stripe-geometry influences cytoskeletal arrangement and focal adhesion formation of neurons and growth cones that determine signal transduction associated with directional neurite growth [25–27]. The stripe-pattern topographies may produce ridge-groove-ridge signals dependent on the pattern dimension that direct growth cone attachment leading to producing oriented and directed growth. The mechanisms by which cells sense stripe-patterned surface contours and translate them into directional growth remains, however, still largely unexplored and are not entirely clear. Our study extends the studies previously reported to indicate that a stripe-pattern determines the growth direction and length of neurites, and the number of neurites per cell depending on the wide of groove and ridge, leading to comprehensive interpretation on the response of neurons to stripe-patterned surface in future.

4. Conclusions

Stripe-patterned polymer films were effective for orientation of neurites extension. Orientation of neurites depended on the pattern width and spacing. These biodegradable patterned films can be used as patterned polymer biomaterials for implants in living body. Patterning of polymers by self-organization can become an effective method for modification of neural implants and contribute to develop regenerative medicine [28–30].

Acknowledgements

This study is supported by Grants-in-Aid from Japan Science and Technology Corporation (JST) and Special Coordination Funds for Promoting Science and Technology.

References

[1] P. Lu, L.L. Jones, E.Y. Snyder, M.H. Tuszynski, Exp. Neulo. 181 (2003) 115–129.
[2] G.A. Silva, C. Czeisler, K.L. Niece, E. Beniash, D.A. Harrington, J.A. Kessler, S.I. Stupp, Science 303 (2003) 1352–1355.
[3] F. Yang, R. Murugan, S. Wang, S. Ramarkrishna, Biomaterials 26 (2005) 2603–2610.
[4] I. Nagata, A. Kawana, N. Nakatsuji, Development 117 (1993) 401–408.
[5] A.M. Rajnicek, S. Britland, C.D. McCaig, J. Cell Sci. 110 (1997) 2905–2913.
[6] A.M. Rajnicek, C.D. McCaig, J. Cell Sci. 110 (1997) 2915–2924.
[7] J.S. Goldner, J.M. Bruder, G. Li, D. Gazzola, D. Hoffman-Kim, Biomaterials 27 (2006) 460–472.
[8] W. Ma, Q.Y. Liu, D. Jung, P. Manos, J.J. Pancrazio, A.E. Schaffner, J.L. Barker, D.A. Stenger, Dev. Brain Res. 111 (1998) 231–243.
[9] J.D. Foley, E.W. Grunwald, P.F. Nealey, C.J. Murphy, Biomaterials 26 (2005) 3639–3644.
[10] A. Tsuruma, M. Tanaka, N. Fukushima, M. Shimomura, e-J. Surf. Sci. Nanotech. 3 (2005) 159–164.
[11] A. Tsuruma, M. Tanaka, N. Fukushima, M. Shimomura, Kobunshi Ronbunshu 61 (2004) 628–633.
[12] J.B. Recknor, D.S. Sakaguchi, S.K. Mallapragada, Ann. N.Y. Acad. Sci. 1049 (2005) 24–27.
[13] P. Clark, S. Britland, P. Connolly, J. Cell Sci. 105 (1993) 203–212.
[14] L. Kam, W. Shain, J.N. Turner, R. Bizios, Biomaterials 22 (2001) 1049–1054.
[15] J. Tan, W.M. Saltzman, Biomaterials 23 (2002) 3215–3225.
[16] J.B. Recknor, J.C. Recknor, D.S. Sakaguchi, S.K. Mallapragada, Biomaterials 25 (2004) 2753–2767.
[17] N. Maruyama, T. Koito, J. Nishida, T. Sawadaishi, X. Cieren, K. Ijiro, O. Karthaus, M. Shimomura, Thin solid films 327–329 (1998) 854–856.
[18] O. Karthaus, N. Maruyama, X. Cieren, M. Shimomura, H. Hasegawa, T. Hashimoto, Langmuir 16 (2000) 6071–6076.
[19] M. Tanaka, M. Takebayashi, M. Miyama, J. Nishida, M. Shimomura, Bio-med. Mater. Eng. 14 (2004) 439–445.
[20] H. Yabu, M. Shimomura, Adv. Funct. Mater. 15 (2005) 575–581.
[21] J. Nemoto, Y. Uraki, T. Kishimoto, Y. Sano, R. Funada, N. Obata, H. Yabu, M. Tanaka, M. Shimomura, Biores. Technol. 96 (2005) 1955–1958.
[22] R.D. Deegan, O. Balajin, T.F. Dupont, G. Huber, S.R. Nagel, T.A. Witten, Nature 389 (1997) 827–830.
[23] M. Nonomura, R. Kobayashi, Y. Nishiura, M. Shimomura, J. Phys. Soc. Jpn. 72 (2003) 2468–2471.
[24] E. Stepien, J. Stanisz, W. Korohoda, Cell Biol. Int. 23 (1998) 105–116.
[25] N.M. Dowell-Mesfin, M.A. Abdul-Karim, A.M.P. Turner, S. Schanz, H.G. Craighead, B. Roysam, J.N. Turner, W. Shain, J. Neural. Eng. 1 (2004) 78–90.
[26] E. Zamir, B. Geiger, J. Cell Sci. 114 (2001) 3583–3590.
[27] C.Y. Xu, R. Inai, M. Kotaki, S. Ramakrishna, Biomaterials 25 (2004) 877–886.
[28] Y. Fukuhira, E. Kitazono, T. Hayashi, H. Kaneko, M. Tanaka, M. Shimomura, Y. Sumi, Biomaterials 27 (2006) 1797–1802.
[29] M. Tanaka, K. Nishikawa, H. Okuba, H. Kamachi, T. Kawai, M. Matsushita, S. Todo, M. Shimomura, Colloids Surf. A., doi:10.1016/j.colsurfa.2005.11.098.
[30] H. Sunami, E. Ito, M. Tanaka, S. Yamamoto, M. Shimomura, Colloids Surf. A., doi:10.1016/j.colsurfa.2005.11.041.

LETTERS AND CORRESPONDENCE

Letters and correspondence submitted for possible publication must be identified as such. Text length must not exceed 500 words and five bibliographic references. A single concise figure or table may be included if it is essential to support the communication. Letters not typed double-spaced will not be considered for publication. Letters not meeting these specifications will not be returned to authors. Letters to the Editor *are utilized to communicate a single novel observation or finding.* Correspondence *is to be used to supplement or constructively comment on the contents of a publication in the journal and cannot exceed the restrictions for* Letters to the Editor. *The Editor reserves the right to shorten text, delete objectional comments, and make other changes to comply with the style of the journal. Permission for publication must be appended as a postscript. Submissions must be sent to Jay Umbreit, MD, PhD, Editor of* Brief Reports/Letters to Editors, American Journal of Hematology, *Winship Cancer Institute, Emory University, 1365-B Clifton Road, Suite B4100, Atlanta, GA 30322 to permit rapid consideration for publication.*

Hb Q India: Is It Always Benign?

To the Editor: Hb Q India is an α chain variant reportedly having no deleterious phenotypic effect [1]. We report 19 cases of Hb Q India detected on HPLC analysis. The MCV was low in five out of 8 Hb Q heterozygotes. The MCV and MCH levels in six Hb Q heterozygotes with β-thalassemia trait were significantly lower than were isolated from Hb Q trait patients ($P < 0.005$). Iron deficiency was found to alter Hb Q levels mildly. Thus, Hb Q trait patients show microcytosis and anemia, which is further accentuated by β-thalassemia trait or iron deficiency.

Subjects included patients visiting hematology department for investigation of anemia from 2001 to 2003. Hemograms were performed on Sysmex Hematology-Analyzer Model K4500 (Sysmex, Mundelein, IL), and Hb variants were quantified by HPLC (Variant™, Bio-Rad, Hercules, CA).

Nineteen cases of Hb Q India were detected from over 4,500 patients investigated, giving an overall prevalence of <0.5%. There were two cases each from 3 families. The clinical features included pallor, generalized weakness, pain in the legs, and breathlessness. In three cases, previous episode(s) of jaundice was present. One patient with associated iron deficiency needed blood transfusion.

TABLE I. Hematological Indices and Hb Q Levels (Mean Values) in Hb Q India Cases*

Parameter	Hb Q Heterozygote	β-Thalassemia trait and Hb Q trait	Iron deficiency with Hb Q trait
No. of patients	8	6	4
Hb (g %)	11.48	10.73	11.0
MCV (FL)	77.2	60.48	67.5
MCH (pg)	26.6	20.0	23.1
MCHC (pg/dL)	34.3	33.1	34.0
RBC count ($\times 10^6$)	4.36	5.37	4.81
Hb Q (%)	18.0	8.9	14.3

*One of the 19 patients was case of G6PD deficiency with Hb Q trait (Hb Q 18.3%).

The different hemoglobins detected on HPLC are listed in Table I. Five out of 8 isolated Hb Q trait patients showed low MCV values. The MCV, MCH, and Hb Q levels in Hb Q heterozygotes with β-thalassemia trait were significantly lower than Hb Q trait alone ($P < 0.005$). Patients of iron deficiency with Hb Q trait also showed lower MCV, MCH, and Hb Q levels, though they were statistically nonsignificant. No homozygous Hb Q India case was detected.

Hb Q India was first described in three Sindhi families (western India) [1]. Subsequently, there have been five reports, which include one of Iranian/French descent [2–4]. The present study is the largest reported from a single institution. The prevalence of Hb Q India (0.4%) was found to be lower than Hb S, Hb E, and Hb D-Punjab in Indian populations [5]. The population prevalence is likely to be even lower. In one patient, jaundice could be explained by G6PD deficiency. The average The Hb Q heterozygotes with concomitant iron deficiency anemia had lower Hb Q levels. Iron deficiency is known to lower Hb A_2 in β-thalassemia trait. G6PD deficiency did not decrease Hb Q level. The high Hb Q level (41.1%) in one case could be due to associated α-thalassemia [2].

The Hb, MCV, and MCH levels in Hb Q trait with and without β-thalassemia trait were lower than reported earlier [2]. In earlier reports, the Hb Q trait patients had normal MCV levels [1–3]. In contrast, seven out of 8 cases in this study have low MCV values. Hb Q heterozygotes also had low Hb level.

Thus, Hb Q heterozygotes may present with microcytosis, mild anemia, and nonspecific symptoms. This is in contrast to previous impressions that isolated Hb Q India is completely benign. Apart from co-existent α-globin/β-globin genotypes, iron deficiency also affects Hb Q levels.

ACKNOWLEDGMENTS

We acknowledge the technical assistance of Mrs. Satyawati Yadav.

I. Panigrahi
J. Bajaj
T. Chatterjee
R. Saxena
M. Mahapatra
H.P. Pati

Department of Hematology, All India Institute of Medical Sciences, Ansari Nagar, New Delhi, India
Published online in Wiley InterScience (www.interscience.wiley.com). DOI: 10.1002/ajh.20240

References

1. Sukumaran PK, Merchant SM, Desai MP, Wiltshire BG, Lehmann H. Hemoglobin Q India (64 (E 13) aspartic acid → histidine) associated with β-thalassemia in three Sindhi families. J Med Genet 1972;9:436–442.
2. Qin WB, Baysal E, Wong KF, et al. Quantities of alpha Q chain variants in heterozygotes with and without a concomitant beta-thalassemia trait. Am J Hematol 1994;45(1):91–93.
3. Schmidt RM, Bechtel KC, Moo-Pen WF. Hemoglobin Q India, alpha 64 (E 13) Asp replaced by His, and β-thalassemia in a Canadian family. Am J Clin Pathol 1976;66:446–448.

4. Dash S, Huisman THJ. Hemoglobin-Q-India (64 (E13) Asp→His) and beta thalassemia: a case report from Punjab (North India). Eur J Haematol 1988;40(3):281.
5. Higgs DR, Thein SL, Wood WG. Distribution and population genetics of the thalassaemias. In: Weatherall DJ, Clegg JB, editors. The thalassaemia syndromes. Oxford, England: Blackwell Scientific Publications; 2001. p 237–284.

Cutaneous Reactions to Imatinib Mesylate Treated by Topical Steroid

To the Editor: Imatinib mesylate is a selective tyrosine receptor kinase inhibitor used to treat CML, Philadelphia-positive acute lymphoblastic leukemia, and gastrointestinal stromal tumors (GIST) [1]. Recently, Rule et al. described two cases of chronic myelogenous leukemia (CML) with severe adverse cutaneous reactions to imatinib mesylate that were controlled by using short-term oral steroid therapy or by reintroducing imatinib mesylate with a gradual escalation in dose [2]. Herein we report two cases of cutaneous reactions to imatinib mesylate that were well-controlled using only topical steroids.

Case 1 involves a 46-year-old man who presented with chronic-phase CML who was started on imatinib mesylate at a dose of 400 mg daily. After 6 weeks of therapy with imatinib mesylate, he developed a scaly pruritic erythema on his face, neck, trunk, and upper limbs (Fig. 1a). These eruptions and the pruritus gradually became aggravated over the next 2 weeks. No other medication could be implicated in these changes. We started to treat him with difluprednate ointment on his body and alclometasone dipropionate ointment on his face, twice daily. The rash quickly resolved without discontinuation of the imatinib mesylate therapy. After 4 weeks of topical steroid treatment, the skin rashes had subsided. However, readministration of imatinib mesylate induced a similar rash again, which was controlled by topical steroids. The patient has been on this treatment for a further 20 months and is showing a good control of the skin rashes using topical steroids only.

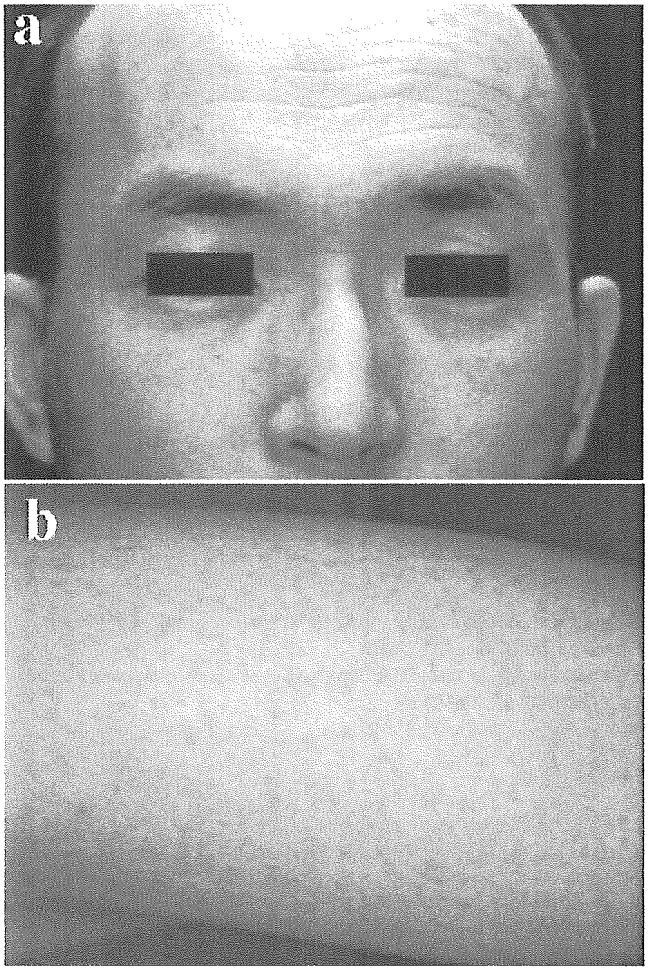

Fig. 1. (a) Scaly pruritic erythemas on the forehead and cheeks. (b) Multiple edematous erythema, 1–3 mm in diameter, scattered on the left upper arm.

Case 2 involved a 43-year-old man with multiple hepatic metastases of GIST who was started on imatinib mesylate at a dose of 600 mg daily. After 9 days, he developed small, finger-tip-sized, multiple edematous erythema on both shins, which spread to over his entire body over the next 2 days (Fig. 1b). We began treating him with diflorasone diacetate ointment twice daily. The rash resolved 2 weeks after topical steroid treatment was initiated without any discontinuation of the imatinib mesylate therapy. The rash was controlled by topical steroid treatment for a further 13 months in conjunction with the imatinib mesylate therapy.

Adverse cutaneous reactions induced by imatinib mesylate are frequent, and various kinds of eruption have been reported. Skin rashes are quite common with the use of this agent [3], and several cases of severe cutaneous reactions, such as erythema multiforme (EM) and Stevens-Johnson syndrome, have been reported [4,5]. These reactions are sometimes life-threatening and require imatinib mesylate treatment to be stopped or oral corticosteroids to be introduced. Cases of severe cutaneous reaction tend to be emphasized in the recent reports [4,5]. The present cases demonstrated that imatinib mesylate can induce not only severe cutaneous reaction but also moderate-type skin rashes as seen in the present reports, which can be controlled with an appropriate topical steroid treatment alone.

Hideyuki Ujiie
Tadamichi Shimizu
Hiroshi Shimizu

Department of Dermatology, Hokkaido University Graduate School of Medicine, Sapporo, Japan
Published online in Wiley InterScience (www.interscience.wiley.com). DOI: 10.1002/ajh.20267

References

1. Demetri GD, von Mehren M, Blanke CD, et al. Efficacy and safety of imatinib mesylate in advanced gastrointestinal stromal tumors. N Engl J Med 2002; 347:472–480.
2. Rule SA, O'Brien SG, Crossman LC. Managing cutaneous reactions to imatinib therapy. Blood 2002;100:3434–3435.
3. Brouard MV, Saurat JH. Cutaneous reactions to STI571. N Engl J Med 2001; 345:618–619.
4. Hsiao LT, Chung HM, Lin JT, et al. Stevens-Johnson syndrome after treatment with STI571: a case report. Br J Haematol 2002;117:620–622.
5. Sanchez-Gonzalez B, Pascual-Ramirez JC, Fernandez-Abellan P, Belinchon-Romero I, Rivas C, Vegara-Aguilera G. Severe skin reaction to imatinib in a case of Philadelphia-positive acute lymphoblastic leukemia. Blood 2003;101:2446.

Hemophagocytosis Evolving Into Acute Lymphoblastic Leukemia

To the Editor: Goldschmidt et al. [1] suggest that the patient reported by them with hemophagocytosis evolving into acute lymphoblastic leukemia showed clonal evolution. However, the karyotype reported during the overtly leukemic phase was 47 XXY, $11p^+$, $18p^+$. This is highly unlikely

to have evolved from a clone with the karyotype shown in a single cell during the hemophagocytic phase, which was reported as 46 XY, $6q^+$, $8q^-$, $11p^+$, $18q^+$.

Although both karyotypes showed $11p^+$, one had addition of material to the short arm of chromosome 18 and the other had addition to the long arm. In addition, it is not at all likely that a more complex karyotype would evolve to a less complex one. It would be possible to postulate that there had been an original clone with 46 XY, $11p^+$, which underwent two different clonal evolutions, that which was detected during the leukemic phase, giving a greater growth advantage.

Barbara J. Bain

Department of Haematology, Imperial College Faculty of Medicine, St Mary's Hospital, London, United Kingdom

Published online in Wiley InterScience (www.interscience.wiley.com). DOI: 10.1002/ajh.20291

Reference

1. Goldschmidt N, Gural A, Kornberg A, Spectre G, Shopen A, Paltiel O. Prolonged fever of unknown origin and hemophagocytosis evolving into acute leukemia. Am J Hematol 2004;76:364–367.

ADVANCED FUNCTIONAL MATERIALS

Preparation of Self-Organized Mesoscale Polymer Patterns on a Solid Substrate: Continuous Pattern Formation from a Receding Meniscus**

By *Hiroshi Yabu** and *Masatsugu Shimomura*

Regular polymer patterns are formed from casting a dilute polymer solution on a solid substrate. Dissipative structures, e.g., convection patterns, fingering instabilities, and so on, are formed in the evaporation process of casting polymer films. Controlled production and manufacturing of patterned polymer films can be achieved when the evaporating solution edge, especially the meniscus region on the casting substrate, is formed under controlled casting conditions. In this report, we describe a computer-controlled apparatus which has two precisely manipulated sliding glass plates. A narrow, thin liquid film of polymer solution with a receding meniscus is continuously supplied from a small gap between two glass plates (one sliding and the other stationary), and a patterned polymer film is subsequently formed on the stationary substrate from the evaporating solution edge. Several types of polymer patterns from various polymers are reproducibly prepared by changing preparation conditions such as sliding speed and polymer concentration.

1. Introduction

Dewetting is a spatio-temporal phenomenon involving the rupture of a thin liquid film on a solid substrate into liquid droplets. Once dewetting occurs in a homogeneous liquid film, randomly formed liquid droplets form irregular figures, such as Voronoi patterns.[1] Dewetting is undesirable in lubrication, lamination, and adhesion applications in industrial coating technology. Therefore, dewetting of polymer melts on solid substrates has been intensively investigated both theoretically[2,3] and experimentally[4–6] in order to fabricate homogeneous polymer thin films. Recently, we have reported that regular polymer patterns are formed from casting a dilute polymer solution on a solid substrate. Dissipative structures formed in the evaporating polymer solution and subsequent dewetting of the polymer film on the substrate cooperatively induce regular pattern formation. Dissipative structures, such as Rayleigh–Bénard convection patterns,[7] fingering instabilities,[8] and other spatio-temporal structures,[9] are formed during the evaporation process of casting polymer films. Fingering instabilities, the so-called "tears of wine" phenomenon caused by Marangoni convection, induce periodic condensation of polymer at the casting solution edge. Subsequently, periodic deposition and highly ordered dewetting of polymer form regular stripe, lattice, and hexagonally arranged dot patterns from polystyrene,[10] electrically conducting polymers,[11] and liquid-crystalline polymers.[12]

Though dissipative structures are typical self-organization phenomena of complexity mediated by many physical and chemical conditions, they can be applied to polymer patterning because of their physical generality. If the patterning process is carried out under controlled casting conditions (controlled with regard to temperature, polymer concentration, solvent, and so on) one can prepare regular polymer patterns reproducibly and continuously. It is noteworthy that the key events inducing pattern formation, fingering instability, and dewetting, occur at the evaporating solution edge. Systematic production and manufacturing of patterned polymer films is possible when the evaporating solution edge, especially the meniscus region on the casting substrate, is formed in a controlled casting process. We report the fabrication of a computer-controlled apparatus which has two precisely manipulated sliding glass plates. A narrow, thin, liquid film of polymer solution with a receding meniscus is continuously supplied from a small gap between two glass plates, and a patterned polymer film is subsequently formed on the stationary substrate from the evaporating solution edge. A fluorescence microscope connected to the apparatus carries out an in-situ observation of the pattern continuously developing at the moving solution edge on the sliding glass plate. Several types of polymer patterns are reproducibly prepared by changing preparation conditions, such as sliding speed and polymer concentration. More complicated patterns are prepared by secondary processing of the patterned films.

[*] Dr. H. Yabu, Prof. M. Shimomura
Nanotechnology Research Center
Research Institute for Electronic Science
Hokkaido University, N12W6, Sapporo, 060-0812 (Japan)
Dr. H. Yabu, Prof. M. Shimomura
Frontier Research System
Institute of Physical and Chemical Research (RIKEN Institute)
1-12, Hirosawa, Wako, Saitama, 351-0198 (Japan)
E-mail: shimo@poly.es.hokudai.ac.jp
Prof. M. Shimomura
CREST, JST
4-1-8, Honmachi, Kawaguchi, Saitama, 332-0012 (Japan)

[**] This work was partly supported by a Grant-in-Aid for Scientific Research from Ministry of Education, Science, Sports and Culture (MEXT) of Japan.

 DOI: 10.1002/adfm.200400315

2. Results and Discussion

To control the pattern-formation process, we fabricated a new apparatus composed of two moving substrate holders and a microscope system (Fig. 1a). A glass plate was attached to a substrate holder, which moved smoothly at a speed set by a computer-controlled driving system. Another glass plate was set on the other substrate holder. The glass plates overlapped by about 3–4 cm and were separated by a narrow gap of 200 μm. Chloroform solutions of polystyrene (PS) and poly(3-hexylthiophene) (PHT) were freshly prepared before casting. Polymer solution (200 μL) were added to the gap between the two glass plates, and the upper glass plate was moved linearly at a speed from 10 $\mu m\,s^{-1}$ to 400 $\mu m\,s^{-1}$. A thin liquid film of polymer solution and meniscus were continuously formed behind the moving edge of the sliding glass plate, and the polymer was continuously deposited on the bottom glass plate following rapid evaporation of solvent at the meniscus.

2.1. Dot, Stripe, and Ladder Structures

Optical microscopy and atomic force microscopy (AFM) images of patterned PS films are shown in Figure 2a. A regular array of micrometer-sized polymer dots was formed when a PS solution of concentration 0.1 $g\,L^{-1}$ was deposited at a sliding speed of 50 $\mu m\,s^{-1}$. The mean diameter of each microdot was 10 μm. AFM measurements showed that the height of the microdots ranged from 50 nm to 100 nm. The spacing between adjacent dots was about 10 μm along the sliding direction and about 2–5 μm perpendicular to the sliding direction. At higher concentration (0.5 $g\,L^{-1}$), micrometer-sized periodic stripes were formed. The stripes were oriented perpendicular to the sliding direction. AFM revealed that the width and height of the stripes were 10 μm and 100 nm, respectively, with a line spacing of 10 μm. Highly uniform ladder-like polymer patterns were formed when a 4.0 $g\,L^{-1}$ solution was used for casting. These "ladder patterns" consisted of thick lines 400 nm high

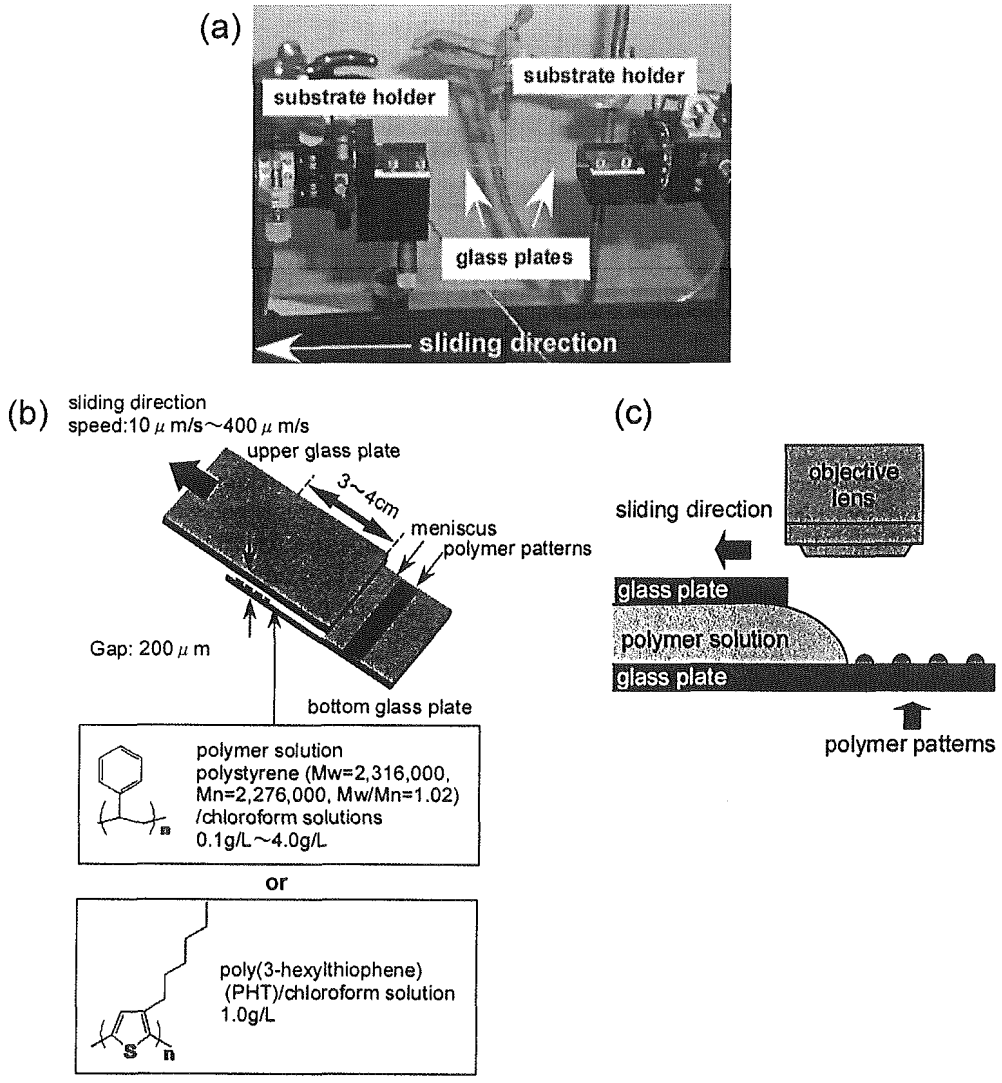

Figure 1. Photographic and schematic illustrations of the experimental set-up.

ADVANCED FUNCTIONAL MATERIALS

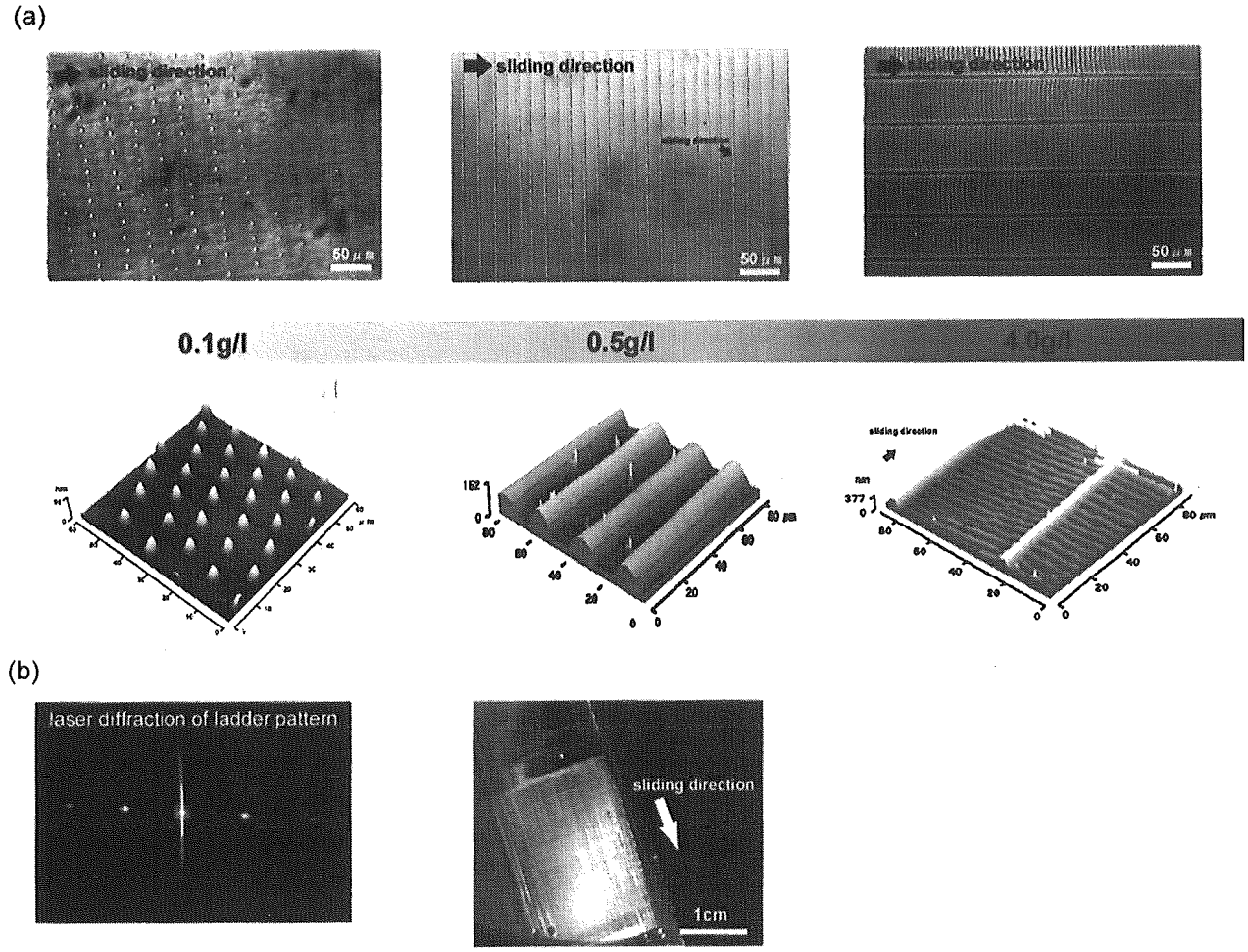

Figure 2. a) Optical (upper row) and atomic force (lower row) microscopy images of polymer patterns prepared from polystyrene solutions. b) The ladder pattern prepared on the glass plate and its laser diffraction pattern.

along the sliding direction, and thin lines 100 nm high perpendicular to the sliding direction.

Figure 2a clearly shows that the concentration of the polymer solution is an important determinant of pattern formation. The array of microdots perpendicular to the sliding direction converts to a single continuous line with increasing concentration. Further increasing the concentration yields new stripes parallel to the moving direction and the formation of ladder patterns. At a sliding speed of 50 $\mu m\,s^{-1}$, 0.3 $g\,L^{-1}$ and 1.0 $g\,L^{-1}$ were the critical concentrations for stripe and ladder formation, respectively, because the coexistence of two patterns (dots and stripes, and stripes and ladders) was found at these two concentrations.

As shown in Figure 2b, glass plates coated by a patterned polymer film showed strong interference colors originating from the microstructures, especially from the ladder pattern. Periodic spots from diffraction of a laser beam (diode-pumped solid-state (DPSS) Nd:YVO_4 laser, $\lambda = 532$ nm) by the ladder-patterned polymer film are also shown in Figure 2b. The two periodic structures formed in the ladder pattern were indicated by two series of diffraction spots crossing each other. Diffraction spots arrayed horizontally were generated by stripes that ran parallel to the sliding direction of the glass plate. These diffractions, with a long spacing, reflect the regular arrangement of the stripes with short repeating period formed perpendicular to the sliding direction. Another series of diffraction spots arrayed vertically, perpendicular to the former series, had a shorter spacing. They were diffracted from another stripe structure formed parallel to the sliding direction, with a long repeating period. This result clearly indicates that the micrometer-scale lattices in the ladder pattern are regular enough to serve as a grating. Thus, highly ordered periodic structures can be easily prepared by our sliding apparatus without conventional lithographic techniques. These micropatterns can be used for optical wave guide arrays, diffraction gratings and photonic bandgap materials.

2.2. Mechanism of Formation of Polymer Patterns

The pattern-formation process was observed at the edge of the upper glass plate by in-situ fluorescence microscopy. Figure 3 shows photographs of the stripe and ladder patterns during their formation. A thin liquid film of polymer solution

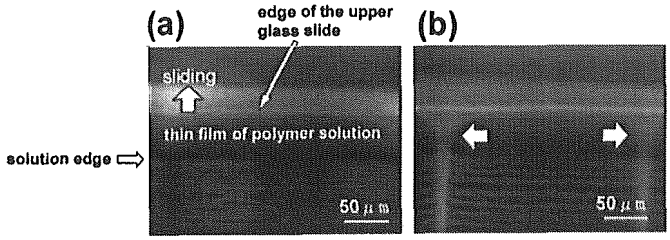

Figure 3. In-situ fluorescence microscopy images of the pattern-formation process. The sliding speed was 50 μm s^{-1} and the solution concentration was a) 0.5g L^{-1} and b) 4.0 g L^{-1}, respectively.

(dark) follows the moving edge (bright) of the upper glass plate, and polymer deposition occurs at the meniscus region of the solution edge (bright). The bright area indicates that the solutes, i.e., polymer and fluorescence probe, are locally condensed. In the case of the 0.5 g L^{-1} solution, polymer was deposited intermittently from the meniscus of the solution to form periodic stripes perpendicular to the sliding direction (Fig. 3a). This type of the periodic deposition is caused by "stick–slip motion", which is often observed in colloidal crystals[13] and is commonly known as the coffee-stain phenomenon.[14] Due to evaporation of solvent at the meniscus, polymer was condensed at the edge of solution.[15] Increasing local viscosity of polymer solution caused by polymer gelation resulted in pinning of the solution edge at the meniscus. After complete deposition of polymer onto the glass substrate, the pinning stress relaxed and the solution edge moved in the sliding direction like a receding tide until the next pinning. The pinning frequency depends on the solution concentration at the meniscus: pinning occurs when the polymer concentration reaches a certain threshold value. Once pinning occurs, the edge of the solution recovers the initial polymer concentration. Repetition of the deposition and recession cycle forms periodic stripes of deposited polymer. Because the time period of the meniscus reaching this threshold was constant, a regular stripe pattern was formed.

In the case of the 4.0 g L^{-1} solution, a series of bright spots emerged along the edge of the glass-slide (Fig. 3b, white arrows). The polymer was deposited from these spots on the substrate to form thick lines parallel to the sliding direction. The spacing between these lines was uniform. This periodic condensation of polymer along the glass edge was caused by convectional flow in the solution, so-called fingering instability.[16] The fingering instability is one of the typical dissipative structures known as the "tears of wine" phenomenon, caused by Marangoni convection and governed by the interaction between surface and interfacial tension. It is known that local condensation of polymer decreases the local surface tension of the solution, and therefore the solution spreads to a region of higher concentration. Convectional flow caused by local fluctuation of surface tension is known as the "solutal Marangoni effect".[17] Local condensation of polymer forms "fingers" by this mechanism. These fingers are fixed on the substrate due to their high viscosity, and regular lines are formed by the continuous deposition of polymer from the fingers. If stick–slip motion and fingering instability occur simultaneously, the ladder pattern is formed.

The dot pattern only formed in dilute solution (e.g., 0.1 g L^{-1}), and was the result of dewetting of the stick–slip stripes. Gelled stick–slip stripes still retained solvent, and as a result, the stripes deformed into dots by Rayleigh instability: the solution of hydrophobic polymer spontaneously ruptured into droplets on the hydrophilic surface to minimize the surface free energy.

2.3. Regulation of Patterns

Figure 4a shows the effect of sliding speed on the spacing of the stick–slip stripes. With increasing sliding speed the spacing of the stripes initially decreases to a minimum at 75 μm s^{-1} and

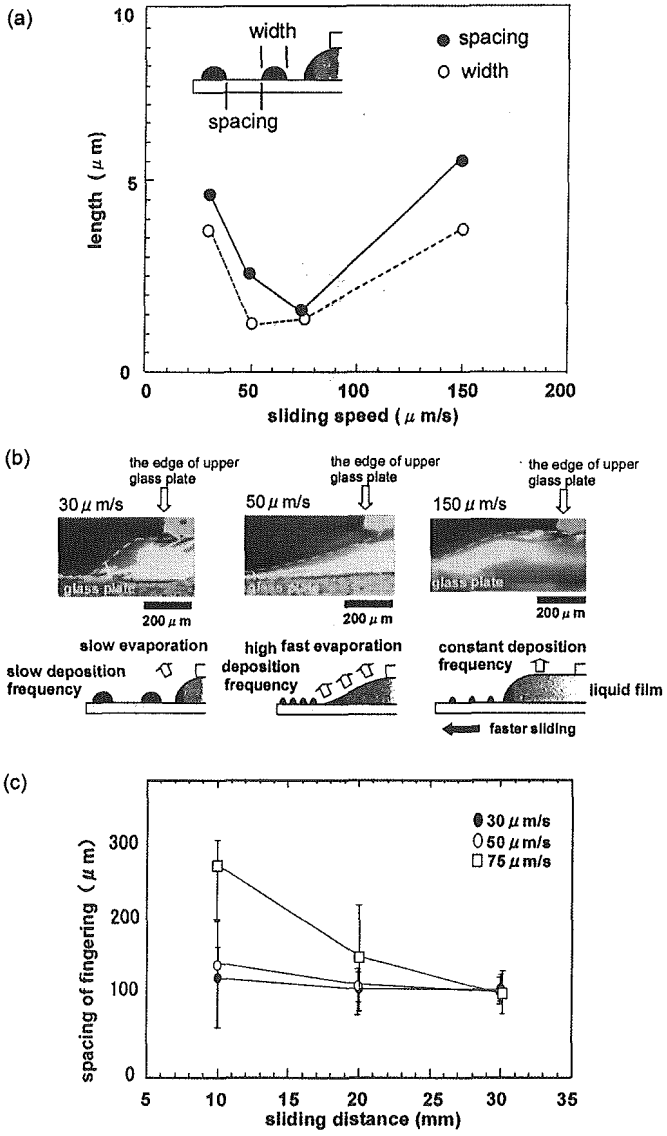

Figure 4. a) Effect of the sliding speed on the spacing of the stick–slip stripe. b) Side view of the receding solution edge at 30 μm s^{-1}, 50 μm s^{-1}, and 150 μm s^{-1}, and their schematic illustrations. c) Plots of distance and fingering spacing at sliding rates of 30 μm s^{-1}, 50 μm s^{-1}, and 75 μm s^{-1}, respectively.

ADVANCED FUNCTIONAL MATERIALS

then increases with increasing speed. The deposition frequency of polymer depends on the evaporation rate of the solvent, and the evaporation rate itself depends on the surface area of the meniscus region where the evaporation events occur. To estimate the area of the meniscus region and its effect on deposition frequency, the side view of the receding meniscus was observed during sliding by in-situ fluorescence microscopy. Figure 4b shows the side views of the receding menisci and their schematic models at various sliding speeds. At low speed (30 $\mu m\,s^{-1}$), the receding contact angle of the polymer solution was about 31° and the meniscus spread about 200 μm from the solution edge to the glass edge. When the sliding speed was increased to 50 $\mu m\,s^{-1}$ the receding contact angle decreased to 11° and the spread of the meniscus expanded to 600 μm. Fluorescence microscopy clearly revealed that the meniscus was deformed and decreased in thickness with increasing sliding speed. At this speed, the enlarged surface area of the deformed meniscus required a shorter time for evaporation than during slower sliding, resulting in an increase in deposition frequency and a corresponding decrease in the spacing of the stripes. Faster sliding (over 75 $\mu m\,s^{-1}$) provided a continuous liquid thin film of polymer solution with its meniscus. At a sliding speed of 150 $\mu m\,s^{-1}$, the receding contact angle was larger than at 50 $\mu m\,s^{-1}$. The shear stress on the meniscus was relaxed and the surface area of the meniscus decreased. Consequently, the deposition frequency decreased and the spacing of stripes increased in proportion to the sliding speed.

The relation between the sliding distance and the fingering spacing is plotted in Figure 4c. In the first stages of sliding, the spacing of the fingers was non-uniform, and decreased as sliding proceeded. Fanton and Cazabat investigated the growth of the fingering instability in a heptane/dodecane system[18] and found that the instability grew until a certain period, after which the system reached a stationary state. In our case, after about 400–600 s (about 18–30 mm on the substrate), the spacing of the fingers converged to 1 μm at any sliding speed. The solvent evaporating only on the solution edge caused no dependence of spacing between fingers on sliding speeds.

2.4. Preparation of Poly(3-hexylthiophene) Micropatterns

One of the advantages of this method is that there is no restriction on polymer materials that can be used for micropatterning. Here, we show the micropatterning of a conducting polymer, PHT. A chloroform solution of PHT was placed in the gap between the glass plates, and one plate was slid at 50 $\mu m\,s^{-1}$. A metallic-looking, colored interference film was obtained (Fig. 5a). Optical microscopy revealed that stripe and ladder patterns were formed (Figs. 5b,c).

Topography and current images simultaneously observed using AFM (Figs. 5d,e) reveal that the micropatterned film was electrically conductiing. The measured conductivity is in the semiconducting regime ($\sigma = 1.3 \times 10^{-4}\ S\,cm^{-1}$), and is the same as that of bulk PHT.[19] This result helps confirm that a wide variety of materials can be patterned using this method.

2.5. Secondary Processing of the Complicated Structures and Patterning on the Curved Surface

The prepared patterns could be peeled off the glass substrate in water. The patterned film (which floats off) could be transferred onto another substrate or patterned film. Figure 6a shows a double-mesh structure of PS prepared by crossing and layering two ladder films.

Furthermore, this method can be utilized for patterning onto curved surfaces. A glass tube with 0.60 mm diameter was inserted into another glass capillary with 0.70 mm internal diameter, and a chloroform solution of PS (1.0 $g\,L^{-1}$) was introduced into the gap between two capillaries. After sliding the inner glass tube, PS microrings were prepared on the outer surface of the inner (0.60 mm diameter) glass tube (Figs. 6b,c). These rings are stick–slip stripes. Patterning of curved surfaces is difficult to achieve by conventional lithographic techniques, but our method can be applied to polymer patterning on substrates of various shapes.

3. Conclusion

We have developed a novel method and an instrument to control mesoscopic patterning from polymer solutions. A polymer solution was introduced into the gap between two glass plates, and the upper glass plate was allowed to slide over the lower. The meniscus of the polymer solution followed the edge of the top glass plate and various polymer patterns were formed on the bottom plate after solvent evaporation. Three different mechanisms, namely, dewetting, stick–slip motion, and fingering instability, gave rise to three types of micrometer-scale patterns with controlled size: dots, stripes, and ladders, respectively. Polymer patterns can be prepared not only on a planar substrate but also on a curved surface. This method is applicable to the patterning of any kind of polymer material, on any scale from the nanometer to the micrometer, because dissipative phenomena and the dewetting process are general physical phenomena of polymer materials. The patterned materials can be applied to photonics,[20] electronics,[21] and biotechnology,[22] and can serve as building blocks for nanometer-scale technologies.[23]

4. Experimental

PS (weight-average molecular weight, $M_w = 2\,316\,000$; number-average molecular weight, $M_n = 2\,276\,000$; $M_w/M_n = 1.02$) and PHT were obtained from Scientific Polymer Products Inc., USA and Aldrich, USA, respectively. Chloroform solutions were prepared with concentrations ranging from 0.1 $g\,L^{-1}$ to 4.0 $g\,L^{-1}$. Glass plates (76 mm × 26 mm) were

obtained from MATSUNAMI, Japan and cleaned by UV/O_3 treatment and ethanol. The water contact angle on the washed glass plate was ca. 0°. The roughness of the glass plates was 2 nm, on average.

Polymer patterns were observed by optical microscopy (BH-2, Olympus, Japan), atomic force microscopy (SPA-400, Seiko Instruments, Japan) and scanning electron microscopy (S-3500, Hitachi, Japan). The process of pattern formation was observed using in-situ fluorescence microscopy using polymer solutions containing 0.05 wt.-% of octadecyl rhodamine B (Molecular Probes, Inc., USA) as a fluorescence probe. The top view and cross-section of the moving meniscus were observed by a revolving objective lens around the glass plates. The pattern-formation process along the evaporating solution edge and the side view of the receding meniscus were stored as digital video images using a video recorder (DV-CAM, SONY, Japan).

The electrical conductivity of the PHT pattern was measured using AFM. The patterned PHT film was fixed on the AFM sample stage with conductive carbon tape (Nitto Denko, Japan). Five volts of bias voltage were applied between the PHT film and a gold-coated AFM tip (SN-AF-01-A, Seiko Instruments Inc., Japan), and the topography and current image were simultaneously obtained.

Received: July 13, 2004
Final version: August 27, 2004

[1] T. G. Stange, D. F. Evans, W. A. Hendrikson, *Langmuir* **1994**, *10*, 1566.
[2] P. E. de Gennes, *Rev. Mod. Phys.* **1985**, *57*, 827.

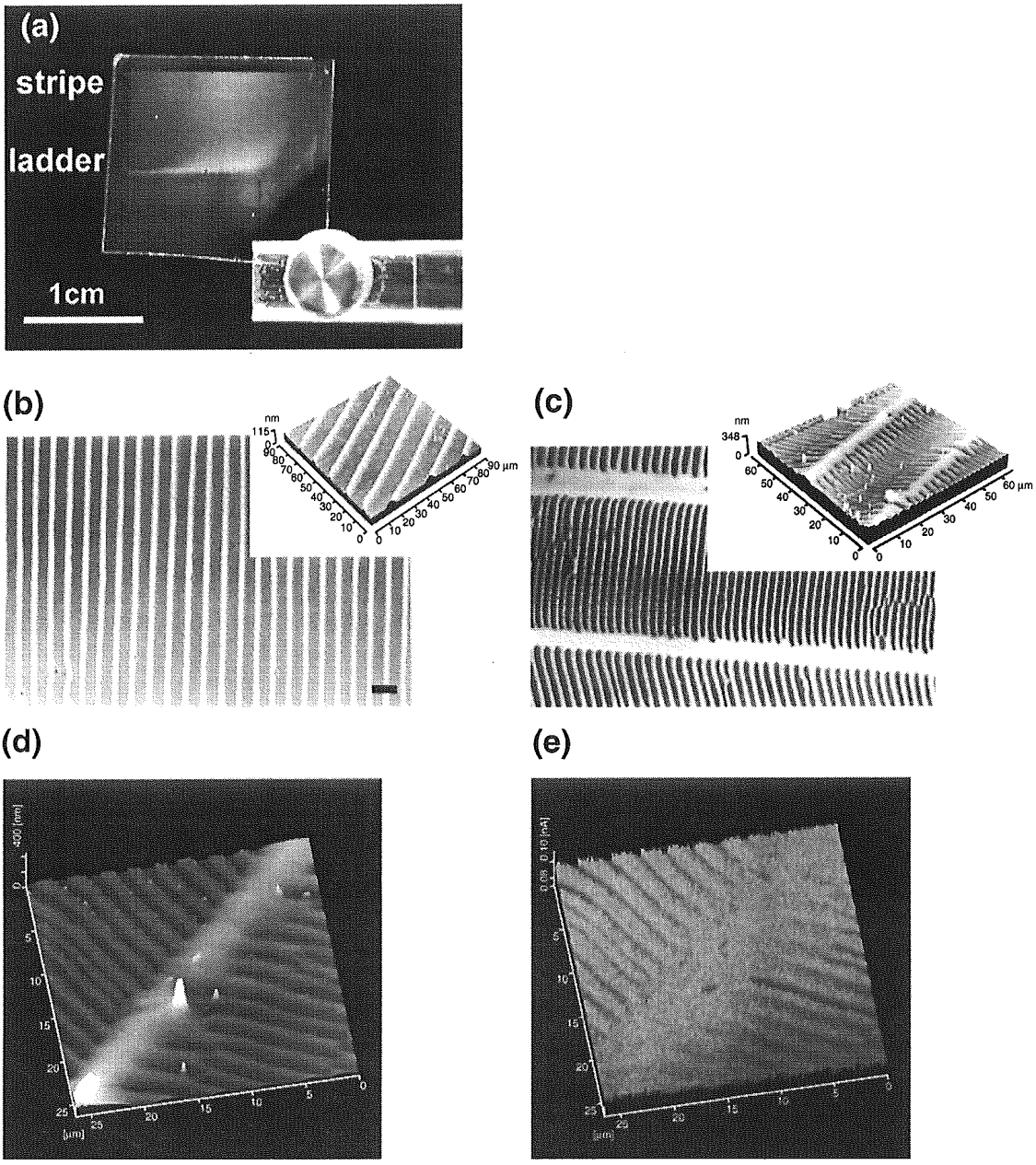

Figure 5. PHT pattern on the glass plate (a). The optical microscopy image of stripe (b) and ladder (c) patterns, respectively. The insets are the AFM images. The topography (d) and current (e) image of PHT ladder pattern simultaneously observed at 5.00 Vcm^{-1} bias voltage.

ADVANCED FUNCTIONAL MATERIALS

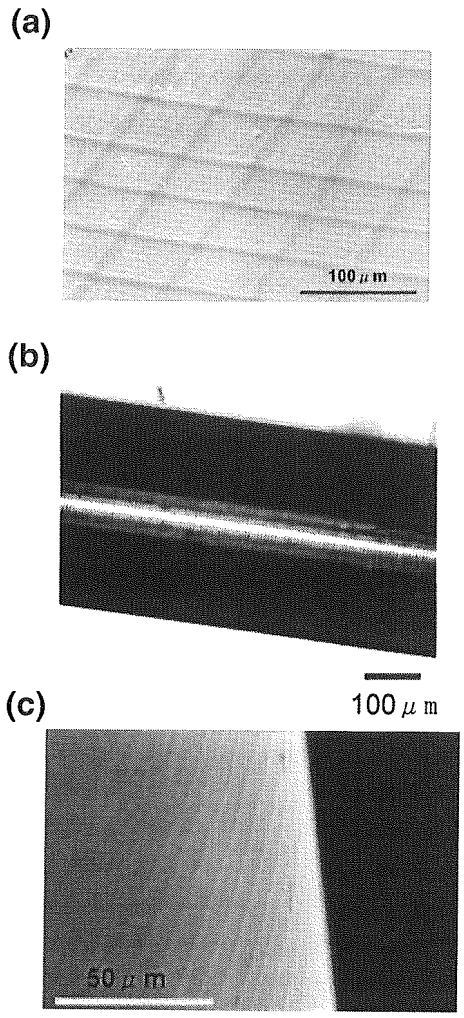

Figure 6. Scanning electron micrograph of a double-mesh structure (a). Optical microscopy image (b) and scanning electron microscopy image (c) of a ring pattern formed on a glass capillary.

[3] R. Khanna, A. Sharma, *J. Colloid Interface Sci.* **1997**, *195*, 42.
[4] A. Sharma, G. Reiter, *J. Colloid Interface Sci.* **1999**, *178*, 383.
[5] G. Reiter, A. Sharma, A. Casoli, M.-O. David, R. Khanna, P. Auroy, *Langmuir* **1999**, *15*, 2551.
[6] C. Yuan, M. Ouyang, J. T. Koberstein, *Macromolecules* **1999**, *32*, 2329.
[7] E. L. Koschmieder, *Adv. Chem. Phys.* **1974**, *26*, 177.
[8] A. M. Cazabat, F. Heslot, S. M. Troian, P. Carles, *Nature* **1990**, *346*, 824.
[9] G. Nicolis, I. Prigogine, in *Self-organization in Nonequiliburim Systems*, Wiley, New York **1977**.
[10] O. Karthaus, L. Grasjo, N. Maruyama, M. Shimomura, *Chaos* **1999**, *9*, 1.
[11] O. Karthaus, T. Koito, M. Shimomura, *Mater. Sci. Eng. C* **1999**, *8–9*, 523.
[12] a) O. Karthaus, N. Maruyama, H. Yabu, T. Koito, K. Akagi, M. Shimomura, *Macromol. Symp.* **2000**, *160*, 137. b) O. Karthaus, H. Yabu, K. Akagi, M. Shimomura, *Mol. Cryst. Liq. Cryst.* **2001**, *364*, 395. c) O. Karthaus, H. Yabu, T. Koito, K. Akagi, M. Shimomura, *Mol. Cryst. Liq. Cryst.* **2001**, *370*, 353.
[13] E. Adachi, A. S. Dimitrov, K. Nagayama, *Langmuir* **1995**, *11*, 1057.
[14] R. D. Deegan, O. Balajin, T. F. Dupont, G. Huber, S. R. Nagel, T. A. Witten, *Nature* **1997**, *389*, 827.
[15] M. Nonomura, R. Kobayashi, Y. Nishiura, M. Shimomura, *J. Phys. Soc. Jpn.* **2003**, *72*, 2468.
[16] N. Maruyama, O. Karthaus, K. Ijiro, M. Shimomura, T. Koito, S. Nishimura, T. Sawadaishi, N. Nishi, S. Tokura, *Supramol. Sci.* **1998**, *5*, 331.
[17] a) R. Vuilleumier, V. Ego, L. Neltner, A. M. Cazabat, *Langmuir* **1995**, *11*, 4117. b) M. Cachile, A. M. Cazabat, *Langmuir* **1999**, *15*, 1515.
[18] X. Fanton, A. M. Cazabat, *Langmuir* **1998**, *14*, 2554.
[19] Molecular Electronic Devices (Eds: F. L. Carter, R. E. Siatkowski), North-Holland, New York **1988**.
[20] J. D. Joannopoulos, R. D. Meade, J. N. Winn, in *Photonic Crystals — Molding the Flow of Light*, Princeton University Press, Princeton, NJ **1995**.
[21] H. O. Jacobs, G. M. Whitesides, *Science* **2001**, *291*, 1763.
[22] E. Ostuni, C. S. Chen, D. E. Ingber, G. M. Whitesides, *Langmuir* **2001**, *17*, 2828.
[23] M. Shimomura, T. Sawadaishi, *Curr. Opin. Colloid Interface Sci.* **2001**, *6*, 1.

Simple Fabrication of Micro Lens Arrays

Hiroshi Yabu*,†,‡,§ and Masatsugu Shimomura†,‡,§

Nanotechnology Research Center, Research Institute for Electronic Science, Hokkaido University, N21W10, Sapporo, 001-0021, Japan, Frontier Research System, Institute of Physical and Chemical Research (RIKEN Institute), 1-12, Hirosawa, Wako, Saitama, 351-0198, Japan, and Core Research for Evolutional Science and Technology (CREST), Japan Science and Technology Agency (JST), 4-1-8, Honcho, Kawaguchi, Saitama, 332-0012, Japan

Received December 6, 2004. In Final Form: January 16, 2005

Microporous polymer films with a hexagonal arrangement of pores were prepared by simple casting of various polymer solutions under humid conditions. Hexagonally packed micropores were prepared by using condensed water droplets as templates on the surface of polymer solutions. Spherical micro lens arrays (MLAs) were fabricated simply by molding from the resulting honeycomb structures. By peeling off the upper layer with adhesive tape, the pillars were severed, forming pins on each layer, and a hexagonal array of pincushion structures was generated by this procedure. Hemispherical MLAs were also fabricated by molding the pincushion structures. The hemispherical MLAs projected clearer miniaturized images than spherical MLAs.

This paper describes the fabrication of micro lens arrays (MLAs) with a hexagonal arrangement. Micro lens arrays are important devices in photonics and electronics. Many applications of MLAs, e.g., coupling lenses for optical telecommunication, light homogenizers in liquid crystalline display (LCD) projectors, image sensors, and others, have already been reported.[1] A simple way to produce MLAs is by molding. Once a suitable template is developed, an MLA can be reproducibly fabricated as a negative mold. The original templates are usually produced by conventional lithographic technologies including the ion exchange technique;[2] modified Lithographie, Galvanoformung, Abformung (LIGA) processes;[3] and anisotropic etching.[4] However, these technologies involve expensive and elaborate multistep processes. Therefore a simple, low-cost method of template fabrication to prepare MLAs is desirable.

The template-directed self-assembly proposed by Whitesides et al. is one of the simple ways of producing MLAs.[5] Microcontact printing and template-directed polymer dewetting on solid substrates have also been used in MLA fabrication.[6] Xia et al. have reported that microsphere arrays self-assembled on a patterned surface were used for MLAs.[7] Additionally, a monolayer assembly of fine polystyrene microspheres prepared on an air−water interface has been used as an MLA.[8] However, these methods all require many steps and prepatterned surfaces prepared by photolithography or soft-lithography. Monodisperse microspheres of suitable materials with high refractive indexes are essential for Xia's method.

It has already been reported that microporous polymer films with a hexagonal arrangement of pores can be prepared by simple casting of various polymer solutions under humid conditions.[9−14] Hexagonally packed micropores in the range of 500 nm to 50 μm were prepared by using condensed water droplets as templates on the surface of polymer solutions. We have found that these micropores have spherical shapes, reflecting the shape of the condensed water droplets. MLAs can be fabricated simply by molding from the resulting honeycomb structures. We report here the straightforward preparation of an MLA from poly(dimethylsiloxane) (PDMS) by molding from the above-mentioned films. Using the spherical pores as templates, a negative mold of the honeycomb film was prepared. Moreover, a hexagonal array of pillar structures was prepared by peeling off the top layer of the honeycomb-patterned film. A hemispherical MLA was prepared by molding the pillar structure. The optical properties of prepared MLAs are discussed below.

After evaporation of solvent under a humid atmosphere, an opaque film was obtained. Typical scanning electron micrographs of the opaque film clearly showed a honey-

* To whom correspondence should be addressed. E-mail: yabu@poly.es.hokudai.ac.jp.

† Nanotechnology Research Center, Research Institute for Electronic Science, Hokkaido University.

‡ Frontier Research System, Institute of Physical and Chemical Research (RIKEN Institute).

§ Core Research for Evolutional Science and Technology (CREST), Japan Science and Technology Agency (JST).

(1) Iga, K.; Kokubun, Y.; Oikawa, M. *Fundamentals of Microoptics*; Academic Press: Tokyo, 1984.

(2) Messerschmidt, B.; Possner, T.; Goering, R. *Appl. Opt.* **1995**, *34* (34), 7825.

(3) Ruther, P.; Gerlach, B.; Göttet, J.; Ilie, M.; Müller, A.; Ossmann, C. *Pure Appl. Opt.* **1997**, *6*, 6643.

(4) Däschner, W.; Long, P.; Stein, R.; Wu, C.; Lee, S. H. *J. Vac. Sci. Technol. B* **1996**, *14* (6), 3730.

(5) Wu, M.-H.; Paul, K. E.; Yang, J.; Whitesides, G. M. *Appl. Phys. Lett.* **2002**, *80* (19), 3500. Wu, H.; Odom, T. W.; Whitesides, G. M. *Adv. Mater.* **2002**, *14* (17), 1213. Wu, M.-H.; Park, C.; Whitesides, G. M. *Langmuir* **2002**, *18* (24), 9312.

(6) Biebuyck, H. A.; Whitesides, G. M. *Langmuir* **1994**, *10* (8), 2790.

(7) Lu, Y.; Yin, Y.; Xia, Y. *Adv. Mater.* **2001**, *13* (1), 34.

(8) Wu, M.-H.; Paul, K. E.; Whitesides, G. M. *Appl. Opt.* **2002**, *41* (13), 2575.

(9) Widawski, G.; Rawiso, M.; François, B. *Nature* **1994**, *369*, 397. Pitois, O.; François, B. *Eur. Phys. J. B* **1999**, *8*, 225. Pitois, O.; François, B. *Colloid Polym. Sci.* **1999**, *277*, 574.

(10) Srinibasarao, M.; Collings, D.; Philips, A.; Patel, S. *Science* **2001**, *292*, 79.

(11) Govor, L. V.; Bashmakov, I. A.; Kaputski, F. N.; Pientka, M.; Parisi, J. *Macromol. Chem. Phys.* **2000**, *201*, 2721. Govor, L. V.; Bashmakov, I. A.; Kiebooms, R.; Dyakonov, V.; Parisi, J. *Adv. Mater.* **2001**, *13* (8), 588.

(12) Karthaus, O.; Maruyama, N.; Cieren, X.; Shimomura, M.; Hasegawa, H.; Hashimoto, T. *Langmuir* **2000**, *16* (15), 6071. Shimomura, M. Hierarchical Structuring of Nanostructured 2-Dimensional Polymer Assemblies. In *Chemistry for the 21st Century*: *Organic Mesoscopic Chemistry*; Masuhara, H., DeSchryver, F. C., Eds.; IUPAC Monograph; Blackwell Science: Oxford, 1999; pp 107−126.

(13) Stenzel, M. H. *Aust. J. Chem.* **2002**, *55*, 239.

(14) de Boer, B.; Stalmach, U.; Nijland, H.; Hadziioannou, G. *Adv. Mater.* **2000**, *12*, 1581. de Boer, B.; Stalmach, U.; van Huttern, P. F.; Melzer, C.; Krasnikov, V. V.; Hadziioannou, G. *Polymer* **2001**, *42*, 9097−9109.

10.1021/la046996z CCC: $30.25
Published on Web 01/29/2005

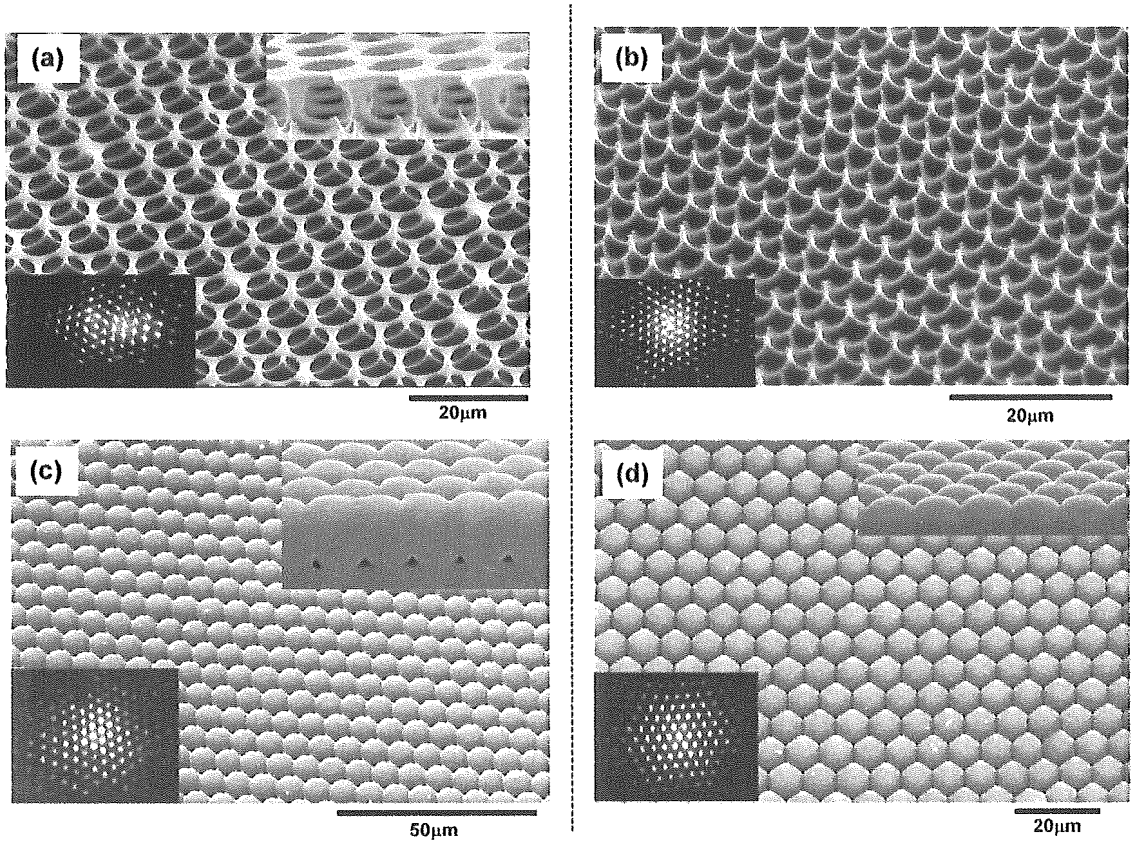

Figure 1. Scanning electron micrograph of porous polymer films and MLAs. (a) A honeycomb film. (b) A pillar structure. (c) A spherical MLA (type A). (d) A hemispherical MLA (type B). Laser diffraction patterns and cross-sectional images are inserted in the lower left and upper right corners of the scanning electron micrographs, respectively.

Scheme 1. Schematic Illustration of MLA Preparation

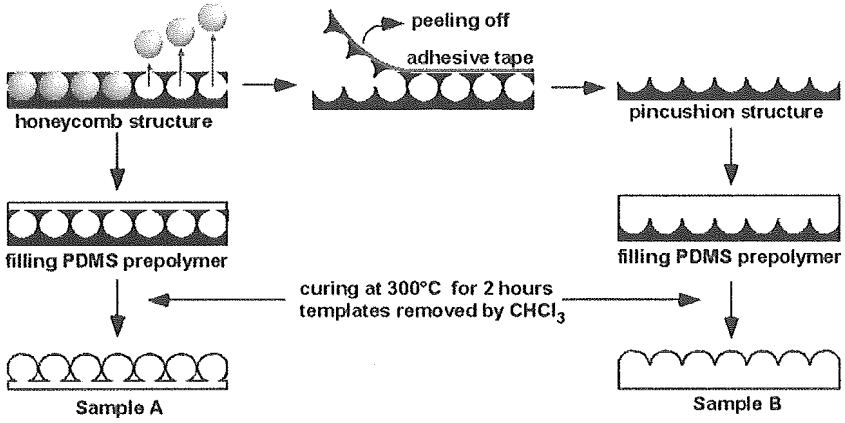

comb-like structure (Figure 1a).[16] This structure reflects the shape and arrangement of condensed water droplets generated on polymer solution surfaces. The pores were connected to each other laterally, and each pore had a spherical shape. The diameters of the honeycomb pores shown in this figure were easily controlled in the range of 500 nm to tens of micrometers simply by changing the volume of solution cast.[15] The honeycomb film showed highly ordered laser diffraction spots, clearly indicating that the arrangement of pores had high periodicity.

A schematic illustration of the preparation procedure is shown in Scheme 1. Honeycomb films were prepared by casting 1.0−5.0 mL of a 5.0 g/L chloroform solution of polystyrene (Chart 1, **1**, Aldrich, $M_w = 280\,000$ g/mol) and amphiphilic copolymer **2** (Chart 1, **1**:**2** = 9:1) in a 9 cm Petri dish. This amphiphilic polymer works as a stabilizer of condensed water droplets and prevents water droplets from fusion. After casting, moist air (relative humidity, ~50%) was applied vertically onto the solution surface. The prepared film was studied by optical (BH-2, Olympus,

Chart 1

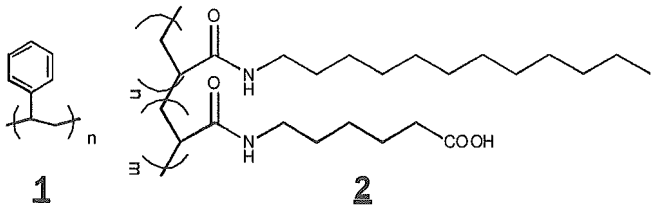

(15) Yabu, H.; Tanaka, M.; Ijiro, K.; Shimomura, M. *Langmuir* **2003**, *19* (15), 6297.
(16) Tanaka, M.; Takebayashi, M.; Yabu, H.; Shimomura, M. *Polym. Prepr. Jpn.* **2003**, *52* (11), 2943.

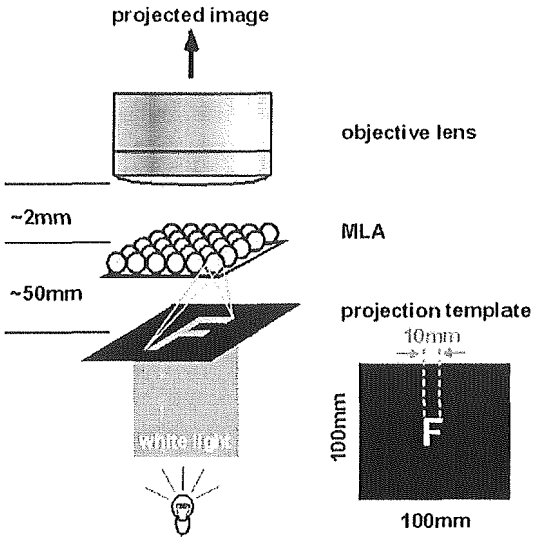

Figure 2. Experimental setup of the projection experiment. The black polymer sheet with a transparent letter F in its center was prepared by a laser printer (Phaser 850, Textronix, U.S.A.)

Japan) and scanning electron microscopy (SEM, S-3500N, Hitachi, Japan) after complete evaporation of solvent and condensed water. Peeled honeycomb films were prepared by peeling off the top layer of honeycomb-structured films using adhesive tape (Scotch Tape, 3M).

The two types of negative molds were prepared from the honeycomb films and peeled honeycomb films, respectively (Scheme 1). PDMS prepolymer (Sylgard184, Dow Corning Inc., U.S.A.) was cast onto a honeycomb film and cured at 300 °C for an hour in an electric oven. The prepared film was then rinsed by chloroform to give a type A MLA. Another type of negative mold was prepared from peeled honeycomb films by casting PDMS prepolymer as before, yielding type B MLAs. The prepared structures were studied by SEM.

The projection experiment was performed with an optical microsope (BH-2, Olympus, Japan) and is depicted in Figure 2. The prepared MLA was fixed on the sample stage of the microscope and illuminated with white light through a projection template, in which a small slit had been made, shaped in the form of the letter F. The size of the optical slit was 10 mm × 10 mm. Miniaturized images of this template were projected through the MLA, and the projected image was observed through the objective lens of the microscope.

The honeycomb-patterned film had a double-layer structure in which the upper layer was connected to the bottom layer by pillars located at the vertexes of the hexagons formed by the pores (Figure 1a).[16] By peeling off the upper layer with adhesive tape, the pillars were severed, forming pins on each layer (Scheme 1), and a hexagonal array of pincushion structures was generated by this procedure. The bottom layer of the film had hexagonally arranged bowl structures (Figure 1b), in which the bowl-shaped dents had submicrometer scale depths and micrometer scale diameters.

PDMS is a suitable material for molding the honeycomb template of polystyrene, for the following reasons: (1) the honeycomb template does not dissolve in the PDMS prepolymer; (2) the refractive index of PDMS is ca. 1.4, which is high enough for the lens material; and (3) PDMS is almost transparent to visible light (wavelengths from 400 to 800 nm). After curing the PDMS prepolymer cast on the template honeycomb film, the polystyrene template was removed by rinsing with chloroform, yielding two-dimensional arrays of spherically shaped (type A) MLAs,

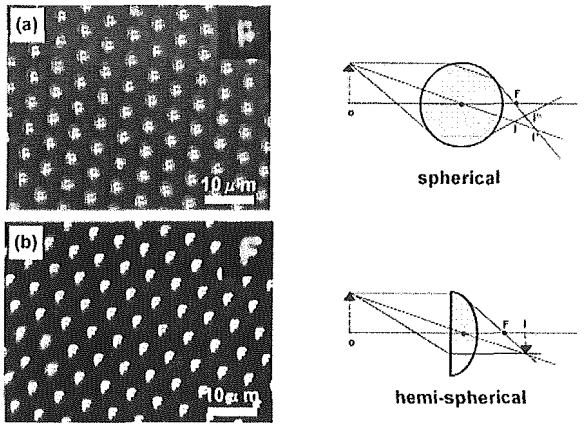

Figure 3. Optical micrograph of projected images through the spherical MLA (type A, (a)) and the hemispherical MLA (type B, (b)). The letter F was clearly observed in the case of the hemispherical lens.

Figure 1c. The PDMS spheres were connected to each other laterally, and the microsphere array was obtained as a free-standing polymer sheet. Hemispherical (type B) micro lenses, Figure 1d, were fabricated from the pincushion structure, with the bowl-shaped dents acting as templates. Highly ordered laser diffraction spots were also observed from the two types of PDMS molds (insets of Figure 1c,d). These results show that each negative mold structure maintained the high periodicity of the original honeycomb template.

A projection experiment was performed with these MLAs using an optical microscope (Figure 2), as follows. The MLAs were placed on the sample stage of the microscope and illuminated with white light from below through a projection template. The projection template was a transparent letter F in a black sheet. A hexagonal array of miniaturized Fs was observed through the objective lens of the microscope when the prepared MLA was inserted under the objective lens. When using the type A MLA, a hexagonal arrangement of bright spots was observed, but the shape of the letter F was not clearly recognized in the spots (Figure 3a). It has been reported that spherical lenses project blurred images because of spherical aberration.[7] In addition, the type A MLA has many focus and image lengths. A hemispherical lens is better suited for the projection of sharp images, since it can focus a light beam originating from a single light source onto a single spot. Using a type B MLA, which has hemispherical lenses, hexagonally arranged Fs were clearly projected (Figure 3b).

We have developed a simple fabrication method to prepare MLAs using self-organized honeycomb-patterned films as templates. Spherical and hemispherical MLAs were prepared by using as templates the original honeycomb films and peeled honeycomb films, respectively. The hemispherical MLA had better projection properties than did the spherical. Our method provides some advantages in the fabrication of MLAs: (1) this method does not require any expensive machinery or materials; (2) the size of the template features is easily controlled (we have already reported[15] that the pore size can be controlled from 200 nm to 100 μm by changing the amount of water used in the process); and (3) our process can be applied to large-scale fabrication of MLAs.

Acknowledgment. This work was partly supported by a Grant-in-Aid for Scientific Research from the Ministry of Education, Science, Sports and Culture (MEXT), Japan.

LA046996Z